

SUPPORTING INFORMATION

From pipemicidic acid molecular salts to metal complexes and BioMOFs using Mechanochemistry

Martin Zábransky^{a,b}, Paula C. Alves^{a,c}, Catarina Bravo^{a,c}, M. Teresa Duarte^{a,d*}, Vânia André^{a,c*}

a) Centro de Química Estrutural, Instituto Superior Técnico, Universidade de Lisboa, Av. Rovisco Pais, 1049-001 Lisboa, Portugal; b) Department of Inorganic Chemistry, Faculty of Science, Charles University, Hlavova 2030, 128 40 Prague, Czech Republic; c) Associação do Instituto Superior Técnico para a Investigação e Desenvolvimento (IST-ID), Av. Rovisco Pais, 1049-003 Lisboa, Portugal; d) Departamento de Engenharia Química, Instituto Superior Técnico, Universidade de Lisboa, Av. Rovisco Pais, 1049-001 Lisboa, Portugal

Structural data

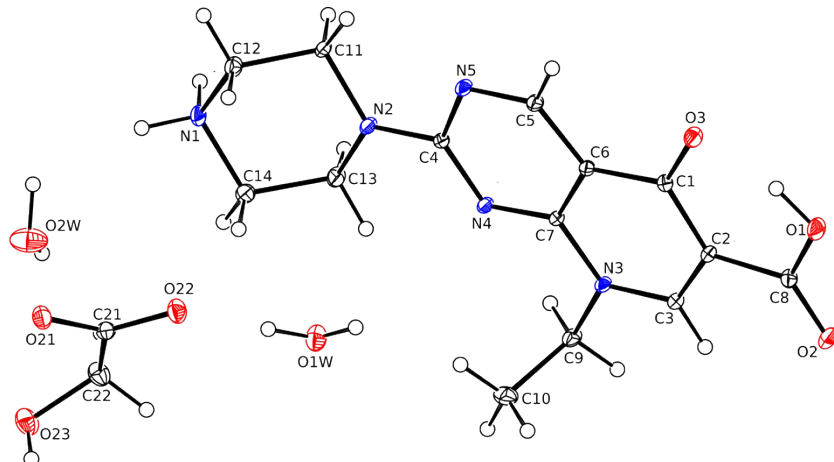


Figure S1. Asymmetric unit in $\mathbf{1} \cdot \text{H}_2\text{O}$. Thermal displacement ellipsoids are plotted at 30 % probability level.

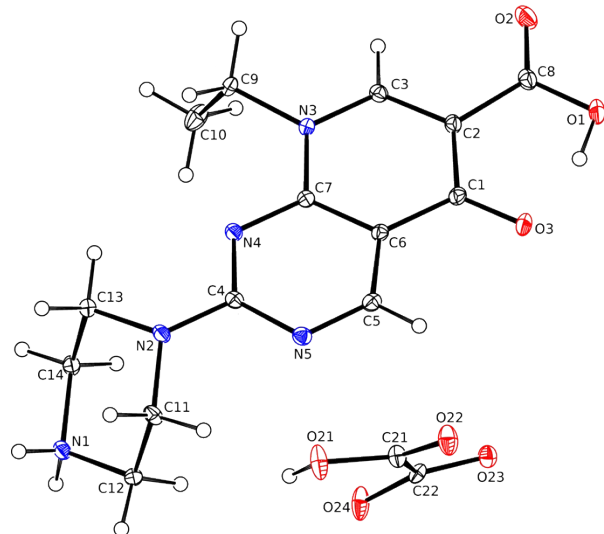


Figure S2. Asymmetric unit in **2**. Thermal displacement ellipsoids are plotted at 30 % probability level.

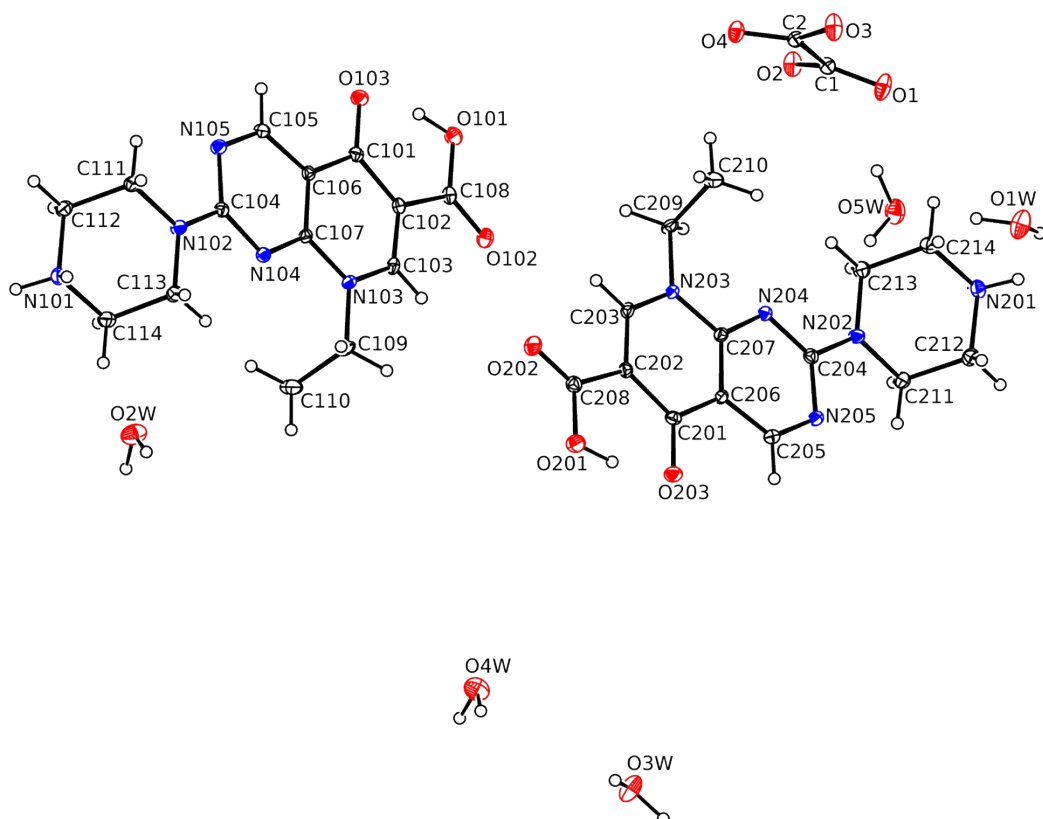


Figure S3. Asymmetric unit in **3·5H₂O**. Thermal displacement ellipsoids are plotted at 30 % probability level.

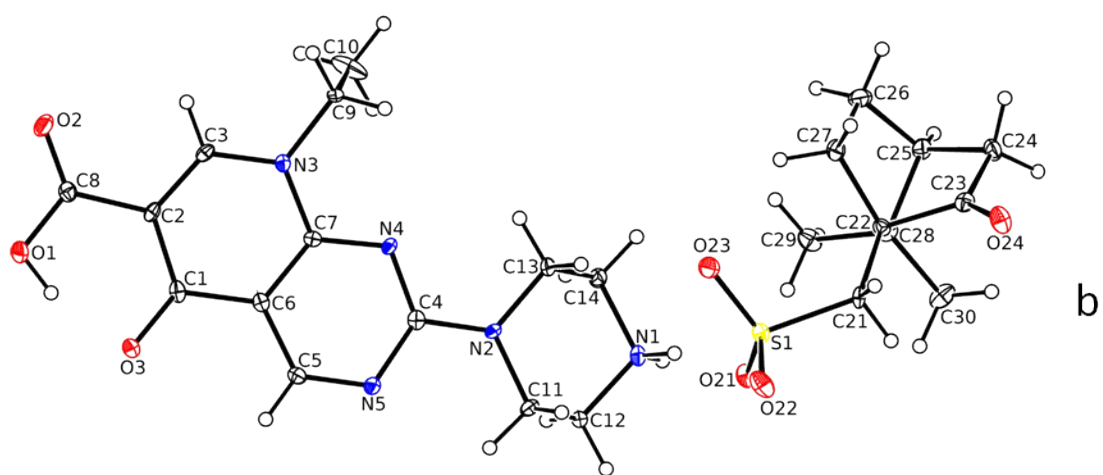
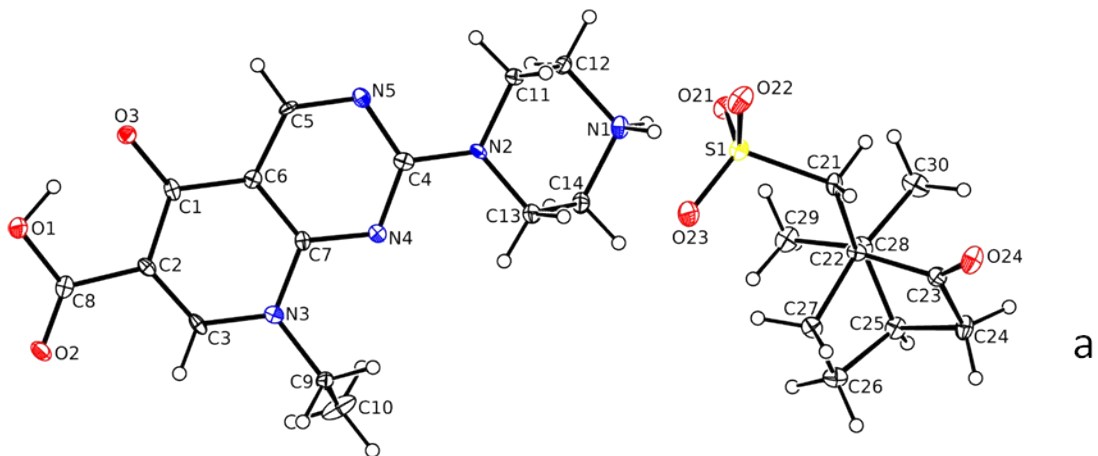


Figure S4. Asymmetric units of (a) **4S** and (b) **4R**. Thermal displacement ellipsoids are plotted at 30 % probability level.

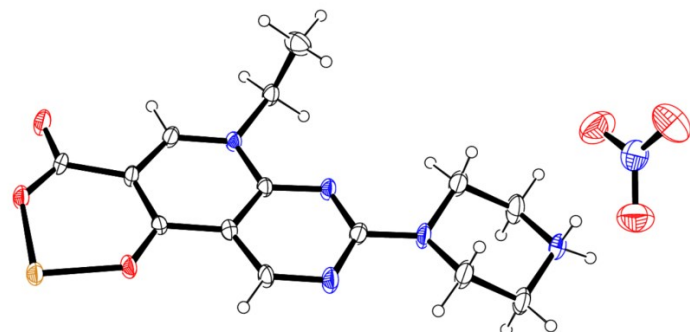


Figure S5. Asymmetric units of **5**. Thermal displacement ellipsoids are plotted at 30 % probability level.

Table S1. Selected bond lengths (\AA) and angles ($^\circ$) for **1·2H₂O**.

C1-O3	1.269(1)	C2-C1-O3	122.5(1)
C8-O1	1.336(2)	C2-C8-O1	114.3(1)
C8-O2	1.209(2)	C2-C8-O2	124.4(1)
C21-O21	1.252(2)	O1-C8-O2	121.3(1)
C21-O22	1.263(1)	C7-N3-C9-C10	-76.3(1)
C21-C22	1.523(2)	C1-C2-C8-O1	-1.1(2)
C22-O23	1.412(2)	C1-C2-C8-O2	178.5(1)
		O23-C22-C21-O22	156.7(1)

Table S2. Selected bond lengths (\AA) and angles ($^\circ$) for **2**.

C1-O3	1.258(2)	C2-C1-O3	122.6(1)
C8-O1	1.328(2)	C2-C8-O1	114.9(2)
C8-O2	1.214(2)	C2-C8-O2	123.5(2)
C21-O21	1.326(2)	O1-C8-O2	121.6(2)
C21-O22	1.201(2)	C7-N3-C9-C10	-87.6(2)
C22-O23	1.242(2)	C1-C2-C8-O1	1.1(2)
C22-O24	1.248(2)	C1-C2-C8-O2	-178.2(2)
C21-C22	1.551(2)	O23-C22-C21-O21	169.2(2)

Table S3. Selected bond lengths (\AA) and angles ($^\circ$) for **3·5H₂O**.

C101-O103	1.256(2)	C102-C101-O103	122.9(2)
C108-O101	1.323(2)	C102-C108-O101	116.0(2)
C108-O102	1.214(2)	C102-C108-O102	123.1(2)
C201-O203	1.262(2)	O101-C108-O102	121.0(2)
C208-O201	1.327(2)	C202-C201-O203	122.9(2)
C208-O202	1.210(2)	C202-C208-O201	114.5(2)
C1-O1	1.238(2)	C202-C208-O202	124.1(2)
C1-O2	1.260(2)	O201-C208-O202	121.5(2)
C2-O3	1.255(2)	C107-N103-C109-C110	76.1(2)
C2-O4	1.243(2)	C101-C102-C108-O101	1.0(2)
C1-C2	1.552(2)	C101-C102-C108-O102	-178.6(1)
		C207-N203-C209-C210	-83.3(2)
		C201-C202-C208-O201	-0.4(2)
		C201-C202-C208-O202	179.5(1)
		O1-C1-C2-O4	-164.1(2)

Table S4. Selected bond lengths (\AA) and angles ($^\circ$) for **4S**.

C1-O3	1.256(7)	C2-C1-O3	122.2(5)
C8-O1	1.326(7)	C2-C8-O1	114.7(5)
C8-O2	1.204(7)	C2-C8-O2	123.7(5)
S1-O21	1.458(4)	O1-C8-O2	121.6(5)
S1-O22	1.459(4)	C22-C21-S1	122.7(4)
S1-O23	1.450(4)	C7-N3-C9-C10	-90.2(6)
		C1-C2-C8-O1	-0.9(8)
		C1-C2-C8-O2	179.7(5)
		C23-C22-C21-S1	-168.8(4)

Table S5. Selected bond lengths (\AA) and angles ($^\circ$) for **4R**.

C1-O3	1.259(6)	C2-C1-O3	123.0(4)
C8-O1	1.322(6)	C2-C8-O1	115.1(4)
C8-O2	1.212(6)	C2-C8-O2	123.3(5)
S1-O21	1.462(4)	O1-C8-O2	121.6(4)
S1-O22	1.458(4)	C22-C21-S1	122.5(4)
S1-O23	1.447(4)	C7-N3-C9-C10	90.3(6)
		C1-C2-C8-O1	0.6(7)
		C1-C2-C8-O2	-179.4(5)
		C23-C22-C21-S1	168.8(4)

Table S6. Selected bond lengths (\AA) and angles ($^\circ$) for **5**.

C(1)-O(3)	1.284(5)	O(3)-C(1)-C(2)	126.2(4)
C(1)-C(2)	1.407(6)	O(3)-C(1)-C(6)	117.6(4)
C(1)-C(6)	1.439(5)	C(2)-C(1)-C(6)	116.2(4)
C(2)-C(3)	1.385(5)	C(3)-C(2)-C(1)	118.8(4)
C(2)-C(8)	1.489(5)	C(3)-C(2)-C(8)	117.4(4)
C(3)-N(3)	1.335(5)	C(1)-C(2)-C(8)	123.8(4)
C(4)-N(4)	1.331(5)	N(3)-C(3)-C(2)	124.5(4)
C(4)-N(2)	1.355(5)	N(4)-C(4)-N(2)	117.6(4)
C(4)-N(5)	1.364(5)	N(4)-C(4)-N(5)	126.6(4)
C(5)-N(5)	1.309(5)	N(2)-C(4)-N(5)	115.8(4)
C(5)-C(6)	1.380(5)	N(5)-C(5)-C(6)	124.8(4)
C(6)-C(7)	1.394(5)	C(5)-C(6)-C(7)	114.9(4)
C(7)-N(4)	1.334(5)	C(5)-C(6)-C(1)	123.3(4)
C(7)-N(3)	1.371(5)	C(7)-C(6)-C(1)	121.7(4)
C(8)-O(2)	1.235(5)	N(4)-C(7)-N(3)	117.4(3)
C(8)-O(1)	1.279(5)	N(4)-C(7)-C(6)	123.3(4)
C(9)-N(3)	1.487(5)	N(3)-C(7)-C(6)	119.3(3)
C(9)-C(10)	1.495(6)	O(2)-C(8)-O(1)	122.4(4)
C(11)-N(2)	1.454(5)	O(2)-C(8)-C(2)	118.8(4)
C(11)-C(12)	1.510(6)	O(1)-C(8)-C(2)	118.8(4)
C(12)-N(1)	1.477(6)	N(3)-C(9)-C(10)	112.4(3)
C(13)-N(2)	1.461(6)	N(2)-C(11)-C(12)	110.1(4)

C(13)-C(14)	1.508(6)	N(1)-C(12)-C(11)	110.8(4)
C(14)-N(1)	1.487(6)	N(2)-C(13)-C(14)	109.9(4)
N(6)-O(4)	1.219(5)	N(1)-C(14)-C(13)	109.5(4)
N(6)-O(5)	1.225(5)	C(12)-N(1)-C(14)	111.3(4)
N(6)-O(6)	1.235(5)	C(4)-N(2)-C(11)	120.7(4)
O(1)-Cu(1)	1.918(3)	C(4)-N(2)-C(13)	121.4(4)
O(3)-Cu(1)	1.891(3)	C(11)-N(2)-C(13)	113.1(4)
Cu(1)-O(3)#1	1.891(3)	C(3)-N(3)-C(7)	119.5(3)
Cu(1)-O(1)#1	1.918(3)	C(3)-N(3)-C(9)	120.9(3)
		C(7)-N(3)-C(9)	119.2(3)
		C(4)-N(4)-C(7)	115.4(3)
		C(5)-N(5)-C(4)	114.9(4)
		O(4)-N(6)-O(5)	121.4(5)
		O(4)-N(6)-O(6)	120.5(5)
		O(5)-N(6)-O(6)	118.0(5)
		C(8)-O(1)-Cu(1)	131.3(3)
		C(1)-O(3)-Cu(1)	126.9(3)
		O(3)#1-Cu(1)-O(3)	180.0
		O(3)#1-Cu(1)-O(1)	87.45(12)
		O(3)-Cu(1)-O(1)	92.55(12)
		O(3)#1-Cu(1)-O(1)#+	92.55(12)
		O(3)-Cu(1)-O(1)#1	87.45(12)
		O(1)-Cu(1)-O(1)#1	180.0

Symmetry transformations used to generate equivalent atoms: #1-x,-y+2,-z+1

Table S7. Cremer-Pople θ angle values [°] and puckering amplitudes Q [Å] of piperazine rings in **1-6**.

Compound	Q [Å]	θ [°]
1 ·2H ₂ O	0.5563(13)	176.64(13)
2	0.5678(17)	174.18(17)
3 ·5H ₂ O	0.5608(17), 0.5494(17)	0.60(17), 177.94(17)
4S	0.561(6)	178.7(5)
4R	0.564(5)	3.4(5)
5	0.566(5)	177.9(5)
6	0.570(6), 0.566(6)	163.7(6), 171.8(6)

Powder X-ray diffraction data – bulk purity

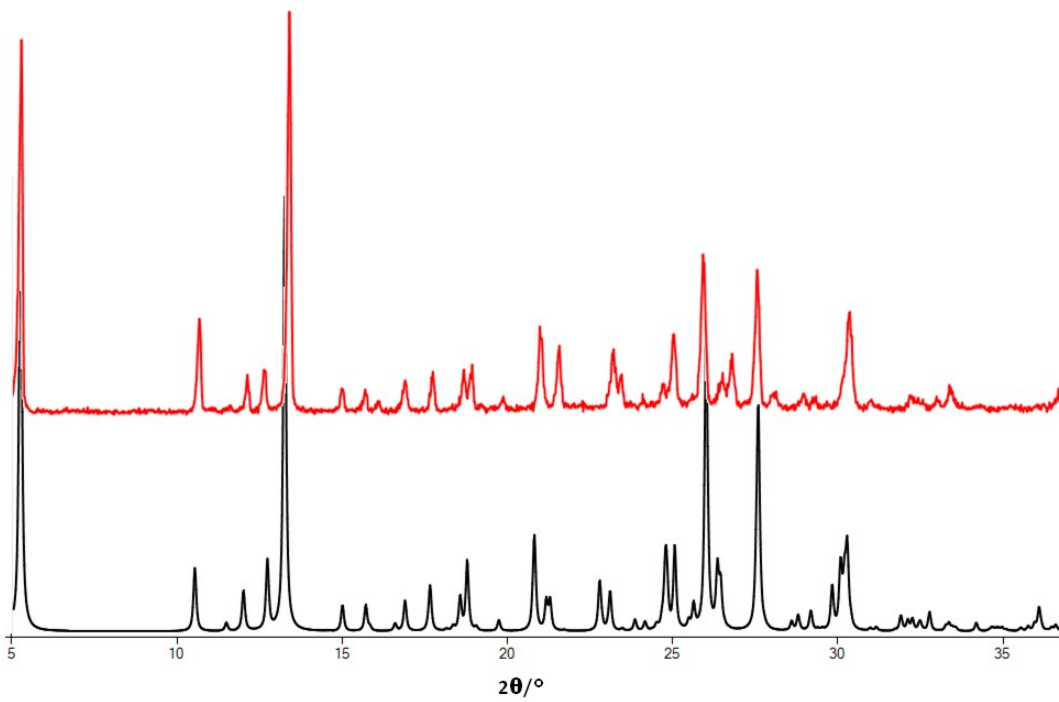


Figure S6. Experimental (red) and simulated (black) powder X-ray diffractograms of **1·2H₂O**.

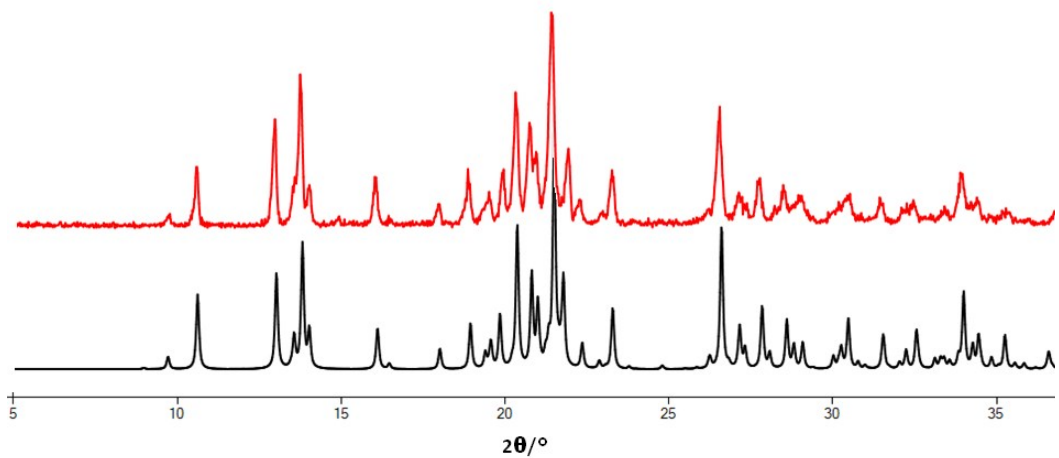


Figure S7. Experimental (red) and simulated (black) powder X-ray diffractograms of **2**.

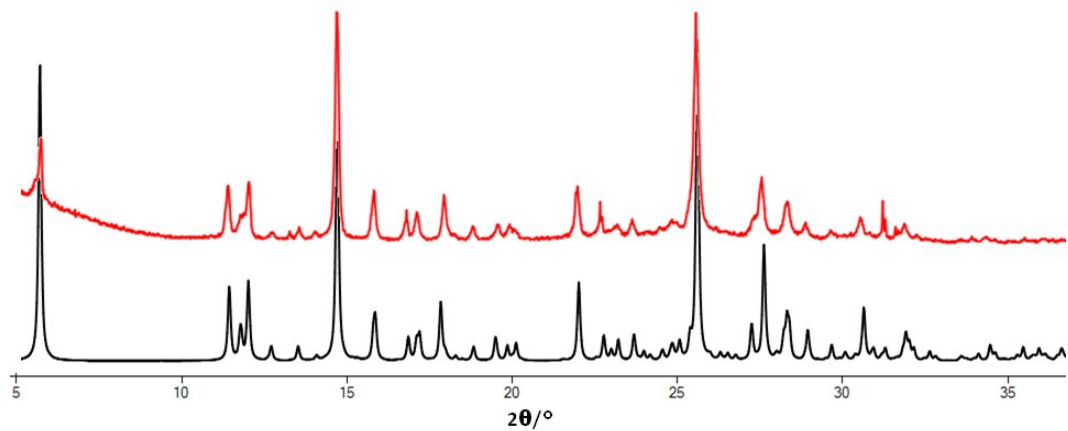


Figure S8. Experimental (red) and simulated (black) powder X-ray diffractograms of **3·5H₂O**.

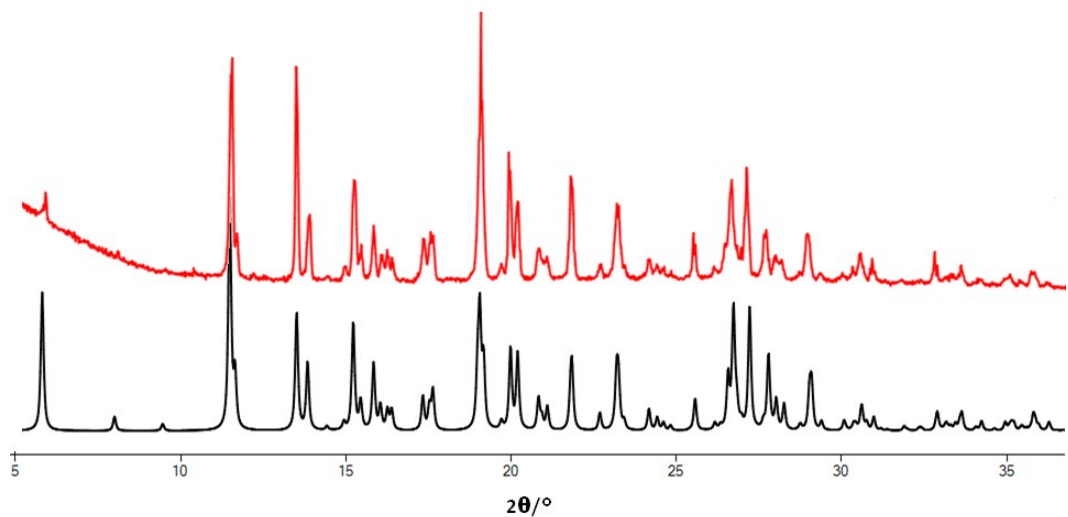


Figure S9. Experimental (red) and simulated (black) powder X-ray diffractograms of **4S**.

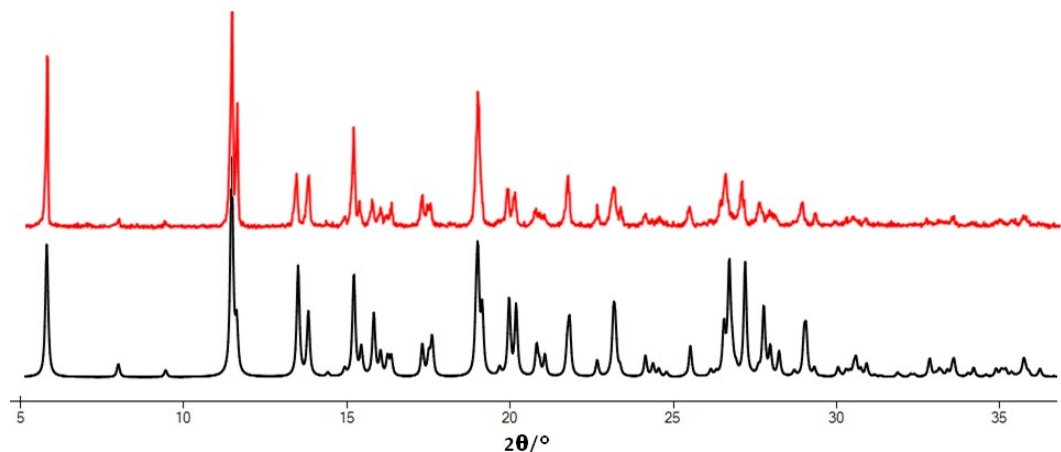


Figure S10. Experimental (red) and simulated (black) powder X-ray diffractograms of **4R**.

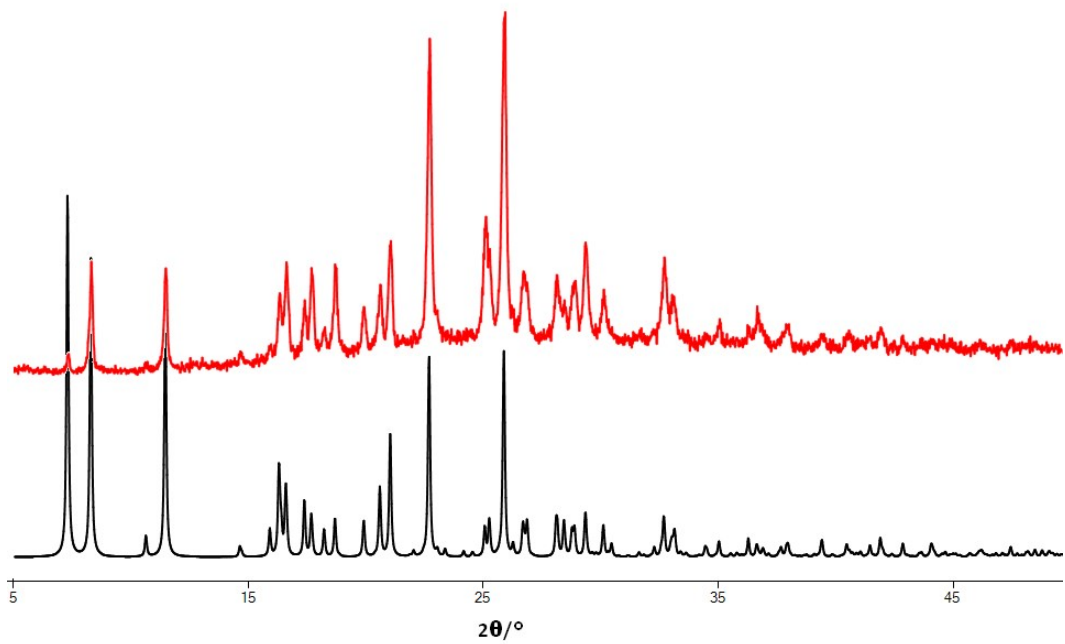


Figure S11. Experimental (red) and simulated (black) powder X-ray diffractograms of complex **5**.

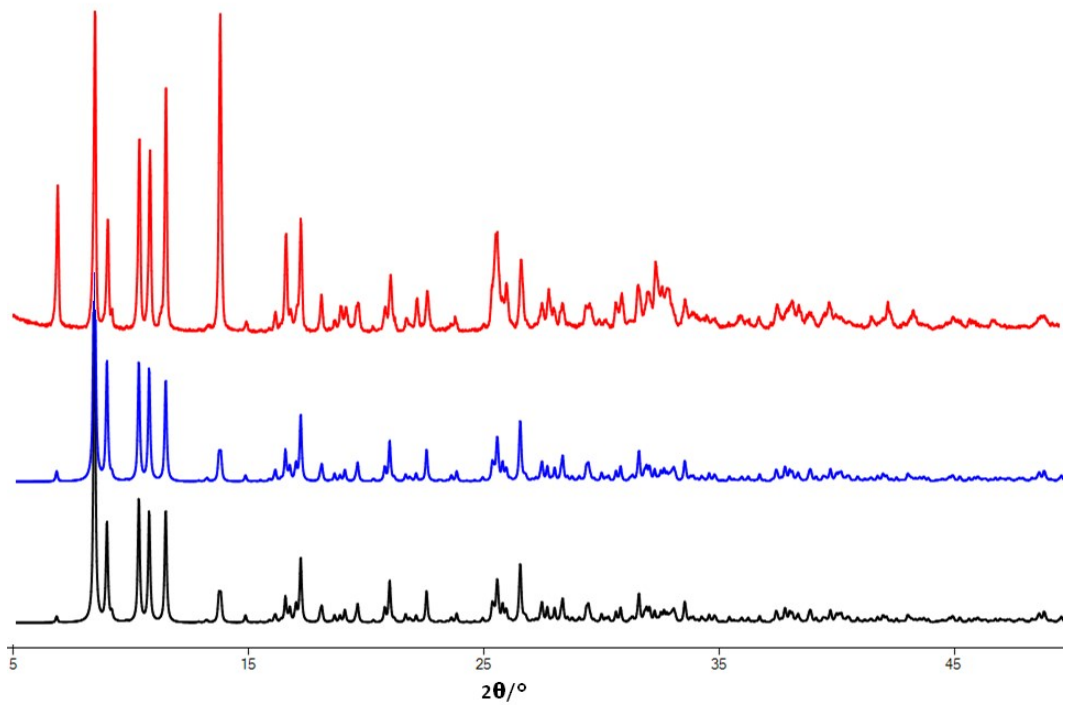


Figure S12. Experimental (red) and simulated powder X-ray (black- GIWNOR; blue- PICWUV) diffractograms of MOF **6**.

Powder X-ray diffraction data – shelf stability

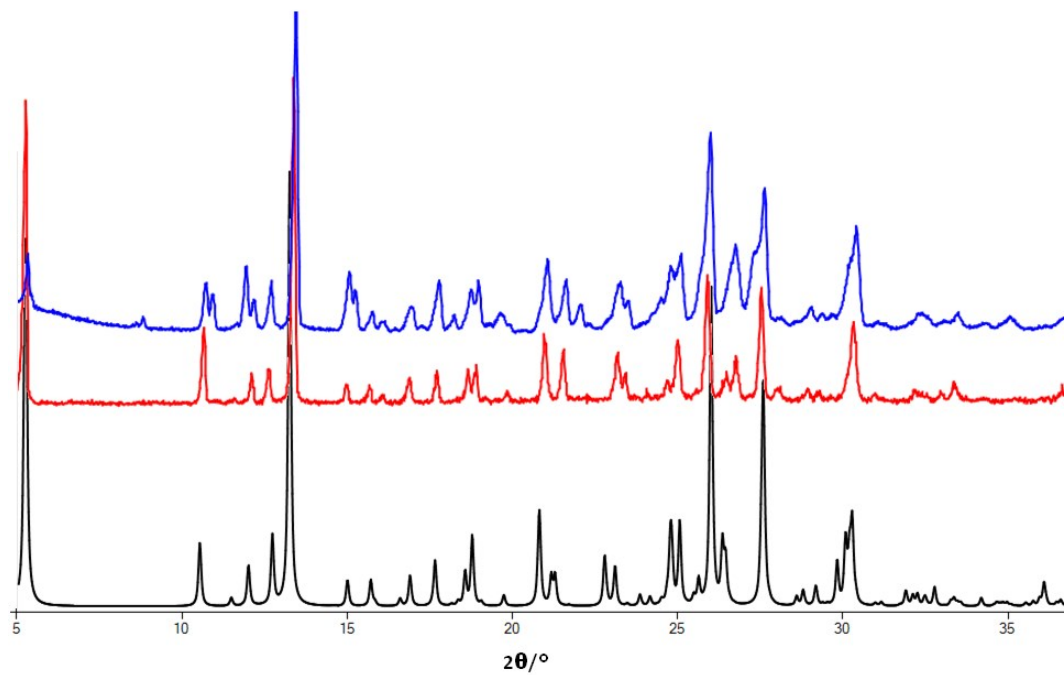


Figure S13. Simulated (black) and experimental (red) powder X-ray diffractograms of **1·2H₂O** after 15 months (blue) on shelf at room temperature.

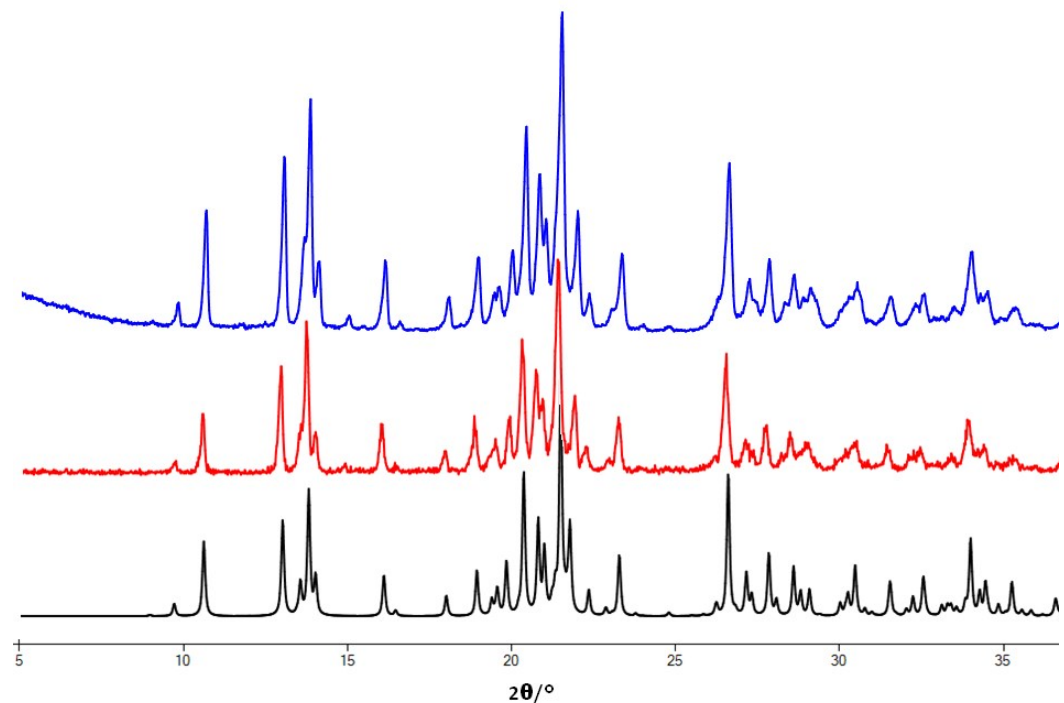


Figure S14. Simulated (black) and experimental (red) powder X-ray diffractograms of **2** after 15 months (blue) on shelf at room temperature.

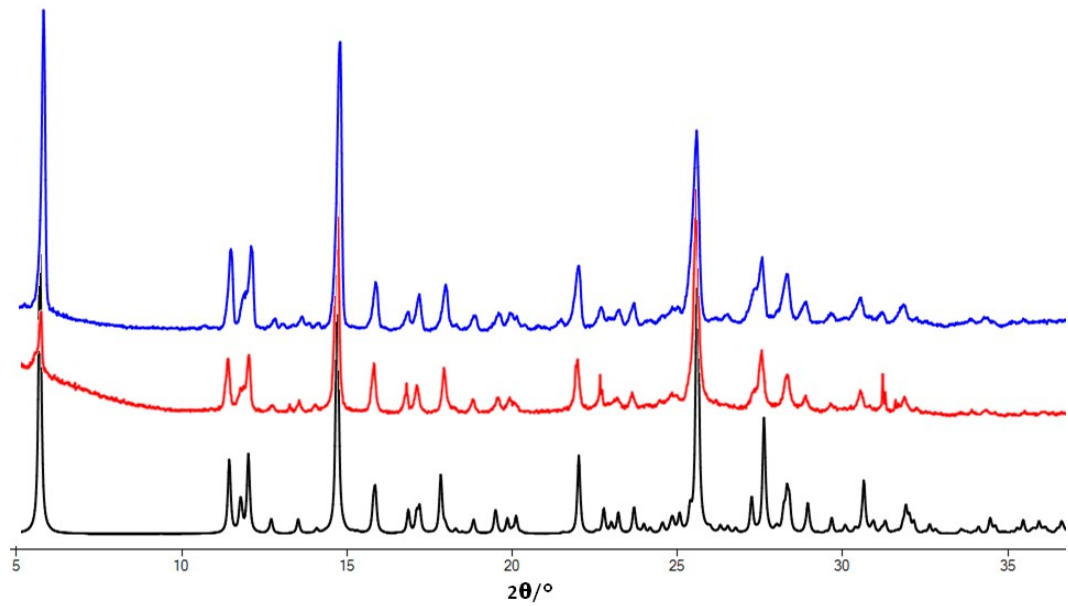


Figure S15. Simulated (black) and experimental (red) powder X-ray diffractograms of **3**·5H₂O after 15 months (blue) on shelf at room temperature.

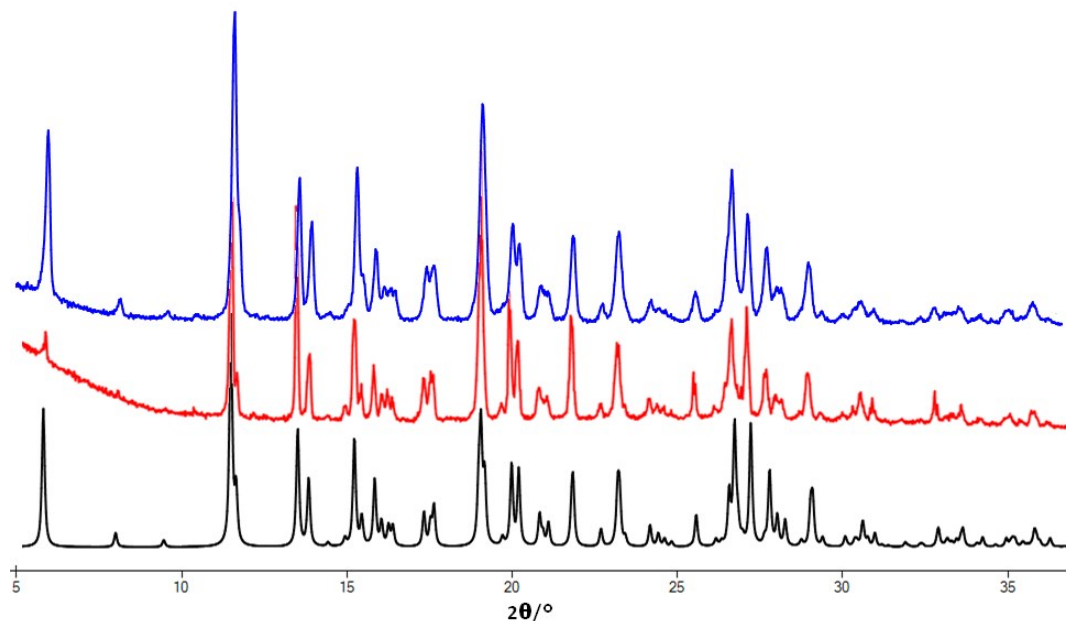


Figure S16. Simulated (black) and experimental (red) powder X-ray diffractograms of **4S** after 15 months (blue) on shelf at room temperature.

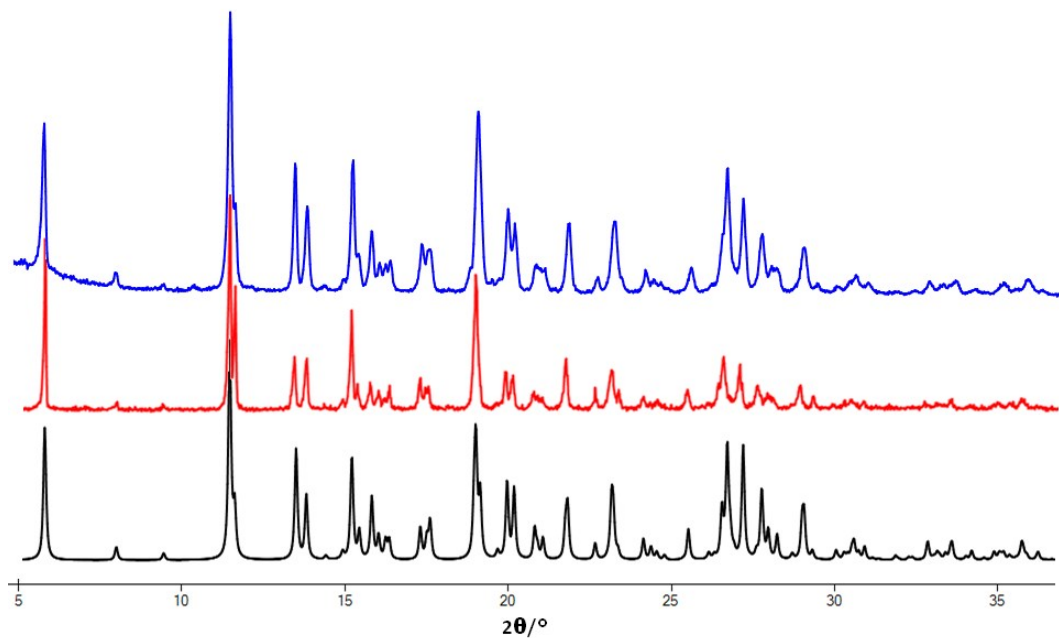


Figure S17. Simulated (black) and experimental (red) powder X-ray diffractograms of **4R** after 15 months (blue) on shelf at room temperature.

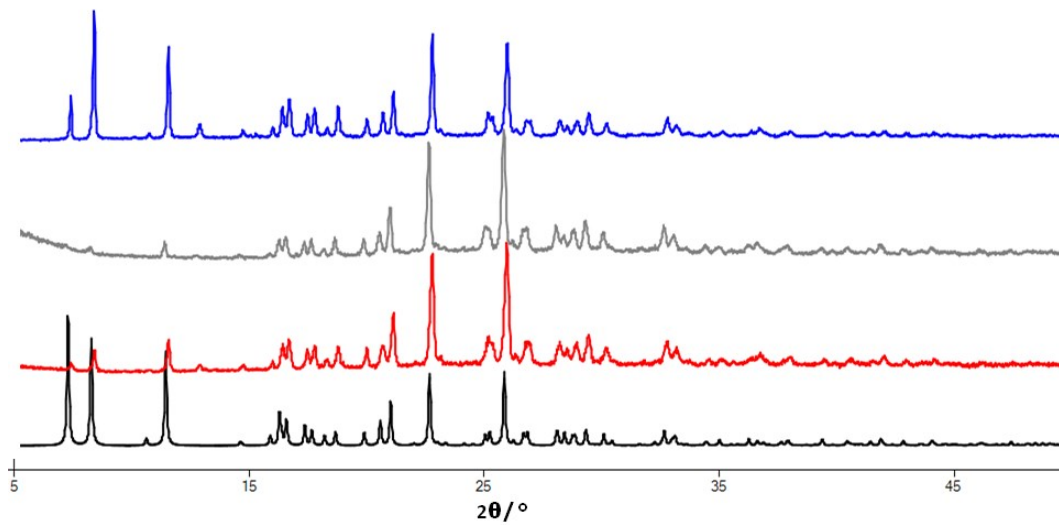


Figure S18. Simulated (black) and experimental (red) powder X-ray diffractograms of **5** after 8 (grey) and 15 (blue) months on shelf at room temperature.

DSC and TGA data

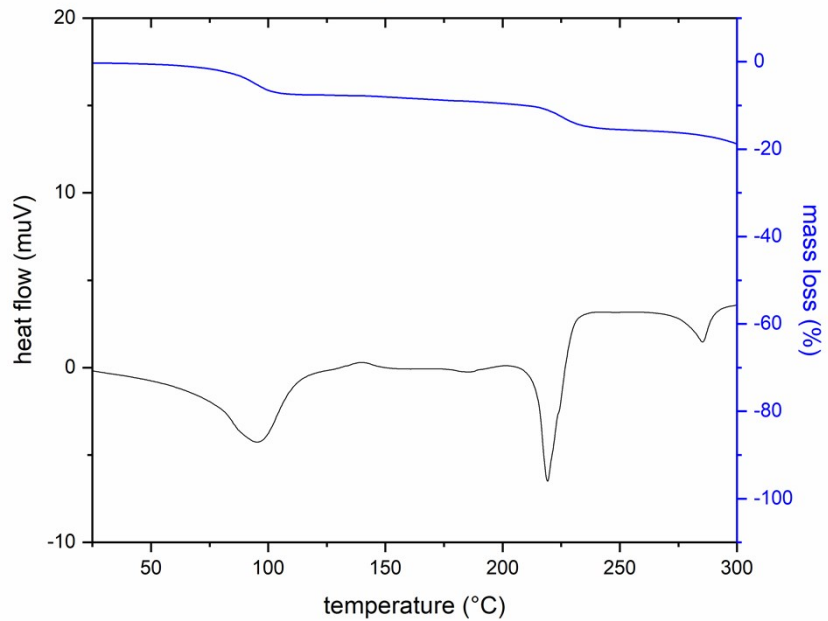


Figure S19. DSC and TGA data for $1 \cdot 2\text{H}_2\text{O}$.

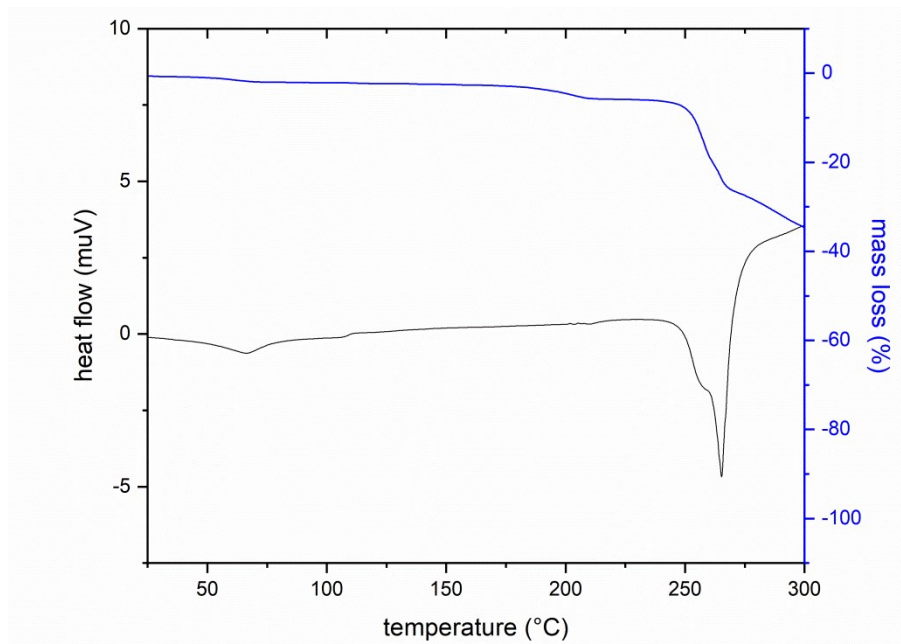


Figure S20. DSC and TGA data for 2 .

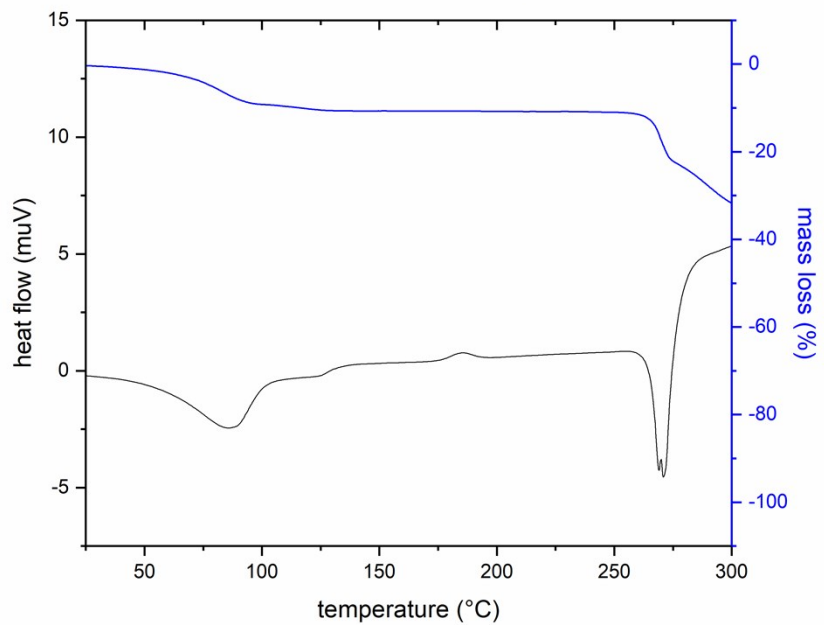


Figure S21. DSC and TGA data for $\mathbf{3} \cdot 5\text{H}_2\text{O}$.

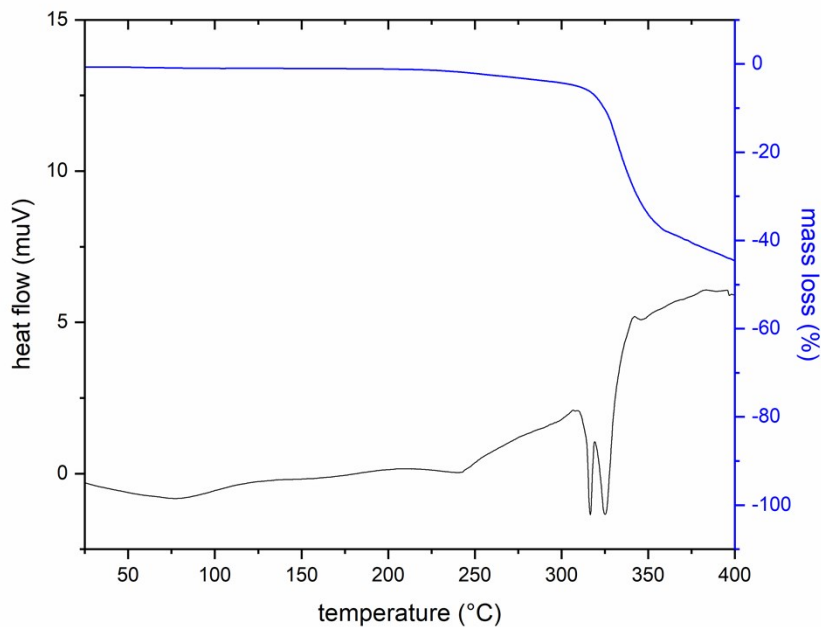


Figure S22. DSC and TGA data for $\mathbf{4S}$.

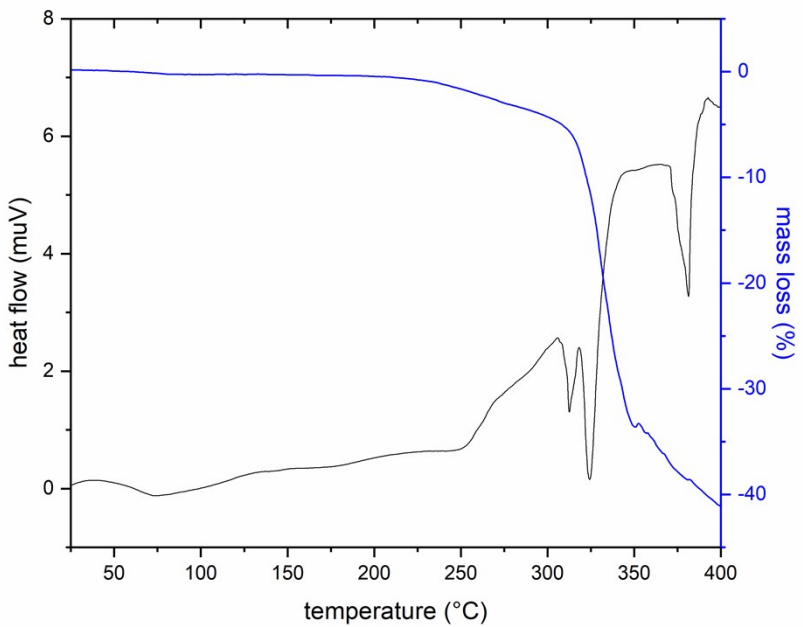


Figure S23. DSC and TGA data for **4R**.

Hot-stage microscopy data

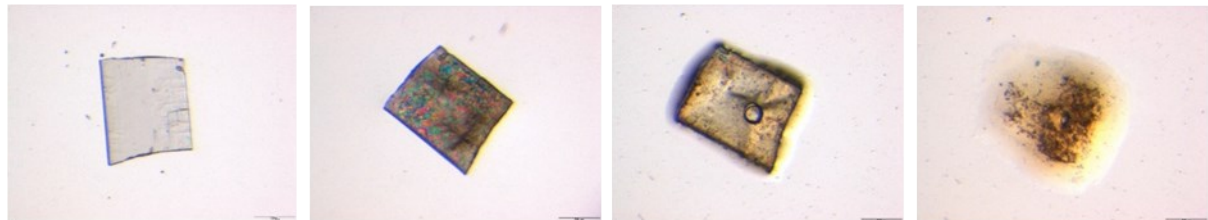


Figure S24. Hot-stage images for **1·2H₂O** (pipemidic glycolate dihydrate) at 23, 98, 219 and 237°C (from left to right).

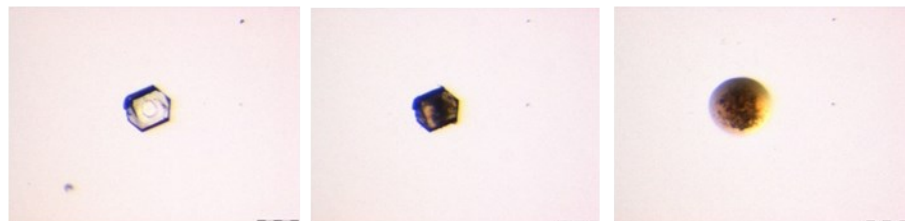


Figure S25. Hot-stage images for **2** (pipemidic hydrogenoxalate) at 23, 252 and 272°C (from left to right).

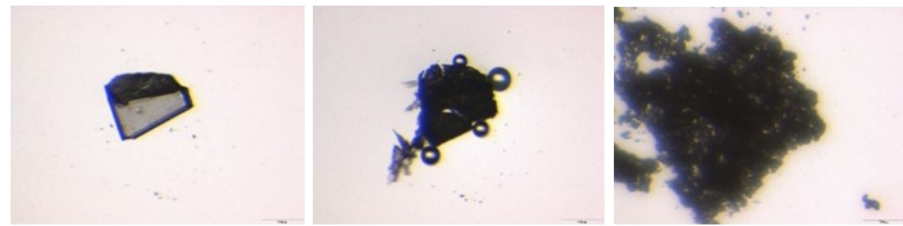


Figure S26. Hot-stage images for **3**·5H₂O (pipemidic hydrogenoxalate pentahydrate) at 21, 100 and 210°C (from left to right).

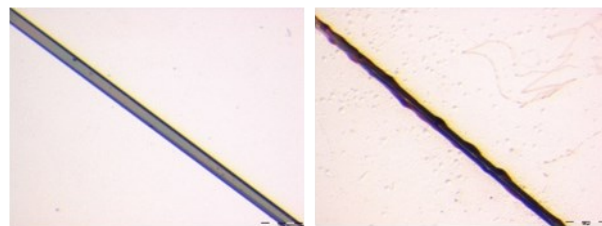


Figure S27. Hot-stage images for **4S** ((S)-camphorsulfonate salt) at 23 and 325°C (from left to right).

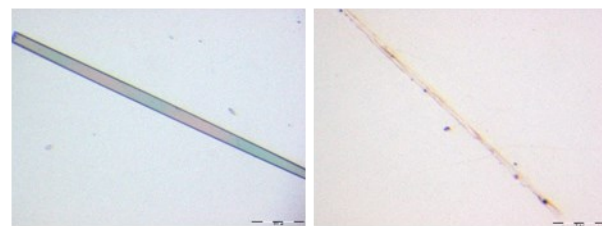


Figure S28. Hot-stage images for **4R** ((R)-camphorsulfonate salt) at 23 and 320°C (from left to right).

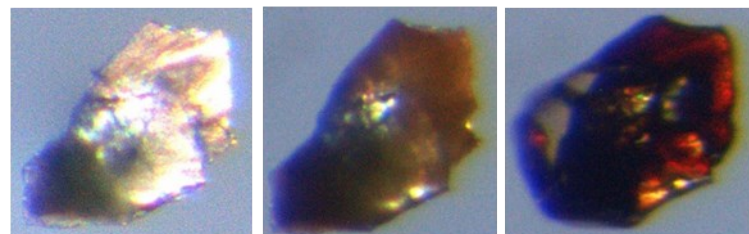


Figure S29. Hot-stage images for **5** at 25, 230 and 298°C (from left to right).

FTIR data

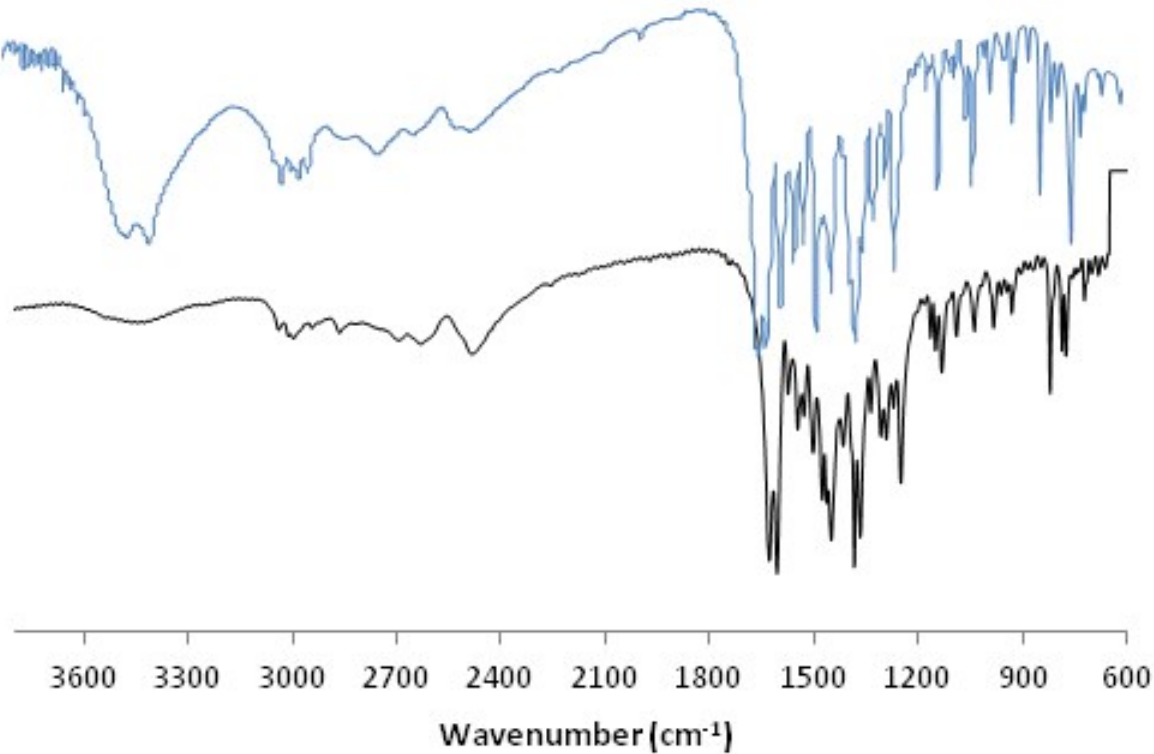


Figure S30. Fourier-transform infrared (FTIR) spectra in KBr pellets of **5** (black) and pipemidic acid (blue).